

RESEARCH

Open Access



Edge-aware nonlinear diffusion-driven regularization model for despeckling synthetic aperture radar images

Anthony Bua^{1*} , Goodluck Kapyela^{1*}, Libe Massawe¹ and Baraka Maiseli¹

*Correspondence:
antwonyb@gmail.com;
gkapyela@gmail.com

¹ Department of Electronics
and Telecommunications
Engineering, College
of Information
and Communication
Technologies, University of Dar
es Salaam, Dar es Salaam 14113,
Tanzania

Abstract

Speckle noise corrupts synthetic aperture radar (SAR) images and limits their applications in sensitive scientific and engineering fields. This challenge has attracted several scholars because of the wide demand of SAR images in forestry, oceanography, geology, glaciology, and topography. Despite some significant efforts to address the challenge, an open-ended research question remains to simultaneously suppress speckle noise and to restore semantic features in SAR images. Therefore, this work establishes a diffusion-driven nonlinear method with edge-awareness capabilities to restore corrupted SAR images while protecting critical image features, such as contours and textures. The proposed method incorporates two terms that promote effective noise removal: (1) high-order diffusion kernel; and (2) fractional regularization term that is sensitive to speckle noise. These terms have been carefully designed to ensure that the restored SAR images contain stronger edges and well-preserved textures. Empirical results show that the proposed model produces content-rich images with higher subjective and objective values. Furthermore, our model generates images with unnoticeable staircase and block artifacts, which are commonly found in the classical Perona–Malik and Total variation models.

Keywords: Image restoration, Multiplicative noise, Noise removal, Regularization, Speckle, SAR

1 Introduction

Synthetic aperture radar (SAR) refers to a classification of radars that uses an antenna mounted on a moving platform, such as an aircraft, to generate detailed images with finer resolution compared with the conventional beam-scanning radars [1]. SAR can operate in different weather conditions, thus making the technology applicable in a wide range of fields: military, oceanography, geology, agriculture, and hydrology [2]. Despite the advantages, SAR imagery suffers from speckle noise (randomly distributed black and white spots in the SAR image) caused by interference of coherent electromagnetic radiation during the imaging process [3, 4]. Speckle noise degrades the visual quality of SAR images, hence making them relatively challenging to interpret

and analyze—a consequence that may limit the application of such images in important scientific and engineering fields.

Scholars have proposed various methods to suppress speckle noise in SAR images. Glaister et al. [5] proposed a Monte Carlo texture-sensitive algorithm to despeckle SAR images by combining two models: local texture and Fisher Tippet logarithmic space speckle distribution. Ni and Gao [6] proposed a despeckling scheme, called the generalized guided filter, where they deduced a nonlinear weight kernel and constructed the guidance image using homogeneity analysis of local regions. Meng et al. [7] introduced a speckle reduction model that focused on the data fidelity term to ensure convexity, and on the Beltrami regularization term to restrain staircase artifacts, while denoising speckles in SAR images. Yu et al. [8] proposed a three-step algorithm (calculation accuracy improvement, iteration, and correction of spreading and blurring of white structures) to suppress speckle noise in SAR images. Many researchers have, also, analyzed various filters, including the Lee Frost, to despeckle SAR images [9–16]. Cao et al. [17] applied deep denoising and convolutional neural networks to detect changes in SAR images. The model was trained to estimate components that contain noise in an image, and these components were then removed to generate better results. In addition, the concept of deep neural network was applied to remove noise on predefined layers of an image. Recently, Gu et al. proposed a two-component deep learning network for restoration of corrupted SAR images. This method gives a proper trade-off between noise reduction and texture preservation, thanks to its spatially adaptive capability [18]. However, the method by Gu et al. suffers from intensity normalization problems, which reduce its performance in images with higher noise density. Other methods for restoring corrupted SAR images have also been proposed in the literature [19–24].

Despite the efforts to despeckle SAR images, the available solutions cannot satisfactorily remove noise while preserving useful features (edges, contours, and textures). Non-linear diffusion offers a promising approach to achieve the two demands and to generate appealing results with higher perceptual and objective qualities. The performance of this denoising framework, however, depends on the regularization prior, which is usually integrated into the divergence term to address the ill-posedness problem caused by insufficient measurements from the observation model (formulation that shows how speckle noise degrades an SAR image). Regularization ensures a proper balance between smoothness of the solution and level of noise in the target image. In this work, we have proposed a regularized nonlinear diffusion model to restore critical features in SAR images while maintaining sufficiently small the amount of noise in the images.

Our research offers three scientific contributions: first, an effective high-order diffusion kernel has been established to regularize noisy images; second, a fractional regularization term that is sensitive to multiplicative noise has been proposed; and third, a mathematical relationship between the proposed method and classical diffusion models (Total variation and Perona–Malik) has been presented. These contributions can advance our current understanding on diffusion processes in image restoration problems. Furthermore, the proposed model gives a proper balance between noise removal and preservation of semantic image features. Moreover, experimental results show that our model remains stable in the iteration system over a longer period. Therefore, the

model can generate appealing images after many iterations, whereas other methods demonstrate poor performance under this condition.

2 Methods

2.1 Problem formulation

In the context of image processing, nonlinear diffusion refers to the process where image regions receive varied denoising levels: stronger diffusion in constant-intensity or nearly flat regions, where noise seems visible naturally; and weaker diffusion near edges and contours [25]. This discriminatory nature of the (nonlinear diffusion) process promotes simultaneous edge recovery and noise removal—an advantage that generates content-rich and perceptually appealing images that can be applied in sensitive applications, including remote detection and analysis of scientific images.

Consider an evolutionary system governed by the time scale, t , which defines smoothness of the evolving (denoising) solution, u . If f denotes the original noisy image, then the nonlinear diffusion process can be described by the general transport equation

$$\frac{\partial u}{\partial t} = \operatorname{div} \left(\frac{\rho'(|\nabla u|)}{|\nabla u|} \nabla u \right) - \lambda R(u, f), \quad (2.1)$$

where $\rho'(\cdot)$ shows the first derivative of the energy functional, $\rho(|\nabla u|)$, that dictates the diffusion process. To achieve desirable solution, scholars recommend $\rho(\cdot)$ to be convex and strictly increasing functional. The term

$$\phi(|\nabla u|) = \frac{\rho'(|\nabla u|)}{|\nabla u|}, \quad (2.2)$$

called diffusivity (conduction coefficient), in (2.1) defines the rate of denoising. The regularization parameter, λ , in (2.1) attempts to establish a trade-off between noise level and smoothness of the evolving solution. Furthermore, the regularization term, $R(\cdot)$, deals with optimum noise minimization relative to the observation (degradation) model, $f = u\eta$, where η denotes the speckle noise power (assumed to be statistically independent of u and f).

For decades, the Perona–Malik nonlinear diffusion model has been widely applied to strategically de-emphasize spurious image features while protecting semantic information [26]. The authors of this model proposed

$$\phi(|\nabla u|) = \frac{1}{1 + \left(\frac{|\nabla u|}{K} \right)^2}, \quad (2.3)$$

where $K \in \mathbb{R}^+$ represents the shape-defining constant. This diffusivity originates from a non-convex energy functional, thus making the Perona–Malik model susceptible to instabilities—a consequence that generates speckle and staircase effects [27]. Rudin et al. [28] proposed a nonlinear diffusion model based on the Total variation of a signal, and the authors used $\phi(|\nabla u|) = 1$ that emulates a convex energy functional. This improved version of the Perona–Malik model produces appreciable results, but suffers

from blocky and intensity reversal artifacts. Both Perona–Malik and Rudin et al. models form the basis of several other nonlinear denoising methods.

Most studies on nonlinear diffusion processes deal with design of the diffusivity and regularization terms to overcome weaknesses of Perona–Malik and Total variation models [29–36]. Despite the convincing performances of the available methods, there has been no standard guidelines to design diffusion coefficients that promote effective noise removal in images. Therefore, variants of Perona–Malik and Total variation lack satisfactory mathematical justifications on why they, in some cases, tend to degenerative solutions or to produce unwanted artifacts.

In this work, we have established a general nonlinear diffusion equation

$$\frac{\partial u}{\partial t} = \operatorname{div} \left(\frac{1}{1 + \sum_{i=1}^N \left(\frac{|\nabla u|}{K_i} \right)^i} \nabla u \right) - \lambda \left(\frac{u - f}{u^\alpha} \right), \tag{2.4}$$

where $\alpha \in \mathbb{R}^+$ represents a tuning parameter. Next, extensive range of experiments were conducted to determine the numerical value of α , and to find the polynomial order of the diffusivity term that can generate optimum denoising results. These experiments aimed at determining numerical values of i and α that neutralize unnecessary artifacts observed in the Perona–Malik and Total variation models. Therefore, we experimentally found that

$$\begin{aligned} \frac{\partial u}{\partial t} &= \operatorname{div} \left(\frac{1}{1 + \frac{|\nabla u|}{K_1} + \left(\frac{|\nabla u|}{K_2} \right)^3} \nabla u \right) - \lambda \left(\frac{u - f}{u^{\frac{1}{6}}} \right), \\ (x, t) &\in \Omega \times (0, T), \\ u(x, 0) &= f, x \in \Omega, \\ \frac{\partial u}{\partial \vec{n}} &= 0, (x, t) \in \partial \Omega \times (0, T), \end{aligned} \tag{2.5}$$

with $\alpha = \frac{1}{6}$ and $i \in \{1, 3\}$, meets our requirements. These numerical values were obtained by running the model in (2.4) through a two-dimensional space of $\{\alpha, i\}$ parameters. Next, optimal values that generate pleasing results were extracted from the space and plugged into the proposed model. The variables in (2.5) are defined as follows: x , two-dimensional spatial coordinates in space; Ω , domain that defines u and f ; T , total time spent by u in the evolutionary system; and \vec{n} , normal vector. Furthermore, empirical results suggest that $K_1 = 1$ and $K_2 = 13$ give denoised images with minimum artifacts.

2.2 Analysis of the proposed model

Performance of the nonlinear diffusion model depends on its corresponding energy functional. Results from previous studies show that most models with convex energy functionals achieve appealing results and converge fast to desirable solutions: detailed images with satisfactory subjective and objective qualities [37]. Some studies, however, argue that non-convex energy functionals can as well generate nonlinear

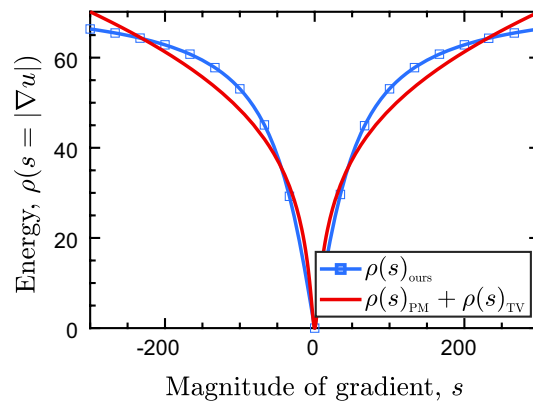


Fig. 1 Our energy functional, $\rho(s)_{\text{ours}}$, versus the combined energy functionals of Perona–Malik and Rudin et al. models, $\rho(s)_{\text{PM}} + \rho(s)_{\text{TV}}$

diffusion models with superior solutions. This situation may be observed in cases when such functionals originate from robust statistics [38, 39].

In this work, we have analyzed the convexity of our energy functional derived from the proposed diffusion equation. Deriving the corresponding energy functional, $\rho(s = |\nabla u|)$, of (2.5), we get

$$\rho(s) = \int \frac{s}{1 + \frac{s}{K_1} + \left(\frac{s}{K_2}\right)^3} d\Omega. \tag{2.6}$$

This equation has a non-trivial solution, and may be solved by relaxing the equation as

$$\rho(s) = \lim_{a \rightarrow 1} \left\{ \int \frac{s}{a + \frac{s}{K_1} + \left(\frac{s}{K_2}\right)^3} d\Omega \right\} \tag{2.7}$$

and by assuming that $s \gg a$. The relaxation of equation (2.7), therefore, evaluates to

$$\rho(s) = \sqrt{K_1} (\sqrt{K_2})^3 \arctan \left(\frac{\sqrt{K_1}}{(\sqrt{K_2})^3} s \right). \tag{2.8}$$

Convexity of $\rho(s)$ in (2.8) can be derived through the derivative test. Therefore,

$$\rho''(s) = \frac{-2K_1^2 K_2^3}{(K_2^3 + K_1 s^2)^2}, \tag{2.9}$$

which gives negative values for $K_1 > 0$ and $K_2 > 0$. Hence, our energy functional is non-convex (Fig. 1). Further analysis of the functional shows that it partly harnesses characteristics from the energy functionals originated from Perona–Malik and Rudin et al. models:

$$\rho(s)_{\text{ours}} \approx \psi(\rho(s)_{\text{PM}} + \rho(s)_{\text{TV}}) \tag{2.10}$$

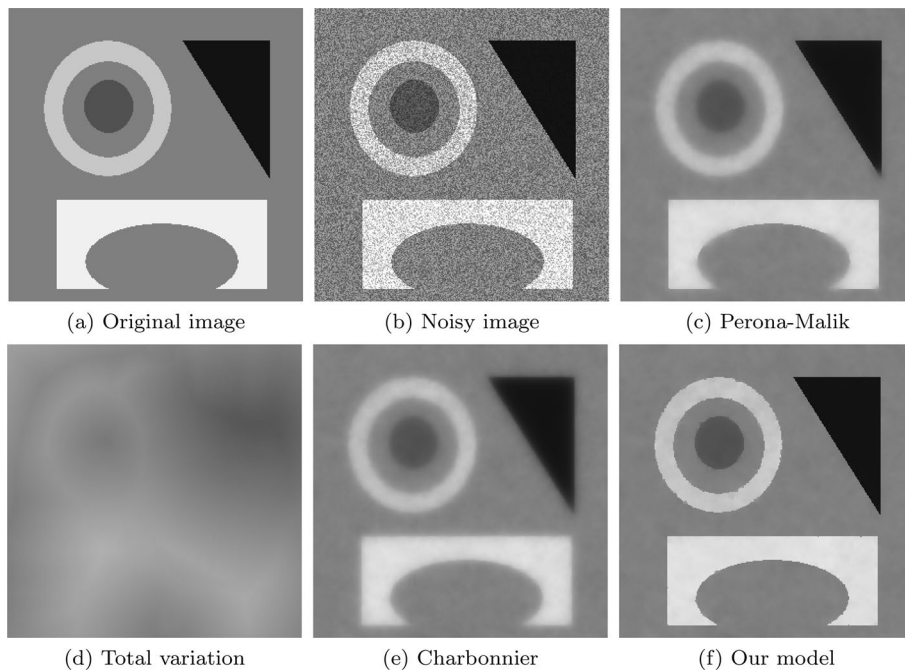


Fig. 2 Denoised images after 15,000 iterations

$$= \psi \left(\frac{K_3^2}{2} \log \left(1 + \left(\frac{s}{K_3} \right)^2 \right) + \frac{s}{K_4} \right), \tag{2.11}$$

where $\{\psi, K_3, K_4\} \in \mathbb{R}^+$; and, $\rho(s)_{PM}$ and $\rho(s)_{TV}$, respectively, denote energy functionals corresponding to Perona–Malik and Rudin et al. models (Fig. 1).

Therefore, strength of the proposed model may be described from the outlined mathematical characteristics of its energy functional, especially that of imitating the combined effects of the Perona–Malik and Rudin et al. energy functionals. Despite the non-convexity nature of our energy functional, we achieved superior denoising results. Even more importantly, the evolutionary system defined by our model remains stable by generating meaningful results over a longer period; conversely, Perona–Malik [26], Rudin et al. [28], and Charbonnier [40] diffusion models generate nearly constant solutions as $t \rightarrow \infty$ (Fig. 2).

2.3 Numerical implementation

The four-point explicit numerical scheme was applied to discretize our model for implementation into the Computer. This scheme has widely been preferred by scholars for its simplicity, lower computational complexity, and reasonable accuracy [41]. Furthermore, an explicit numerical scheme may guarantee stability under Courant–Friedrichs–Lewy condition [42], which requires restriction of time-step, Δt , of the evolutionary system to within the range $[0, 0.25]$.

The numerical scheme used in our work contains four conduction coefficients in the North (N), South (S), East (E), and West (W) directions, respectively labeled as $cN_{i,j}$, $cS_{i,j}$, $cE_{i,j}$, and $cW_{i,j}$, where (i, j) denotes coordinates of the discretized space corresponding

to the continuous spatial space x . The discrete gradients of u along the four directions of the scheme can be defined as $\Delta_N u_{i,j} = u_{i-1,j} - u_{i,j}$, $\Delta_S u_{i,j} = u_{i+1,j} - u_{i,j}$, $\Delta_E u_{i,j} = u_{i,j+1} - u_{i,j}$, and $\Delta_W u_{i,j} = u_{i,j-1} - u_{i,j}$.

Navigating through the diffusivity of (2.5), the discrete versions of the conduction coefficients and divergence term become

$$c^{\Theta_{ij}} = \left\{ \frac{1}{1 + \frac{\Delta_{\Theta} u_{i,j}}{K_1} + \left(\frac{\Delta_{\Theta} u_{i,j}}{K_2}\right)^3} \right\}_{\Theta \in \{N, S, E, W\}} \tag{2.12}$$

and

$$\text{div}_{i,j} = \sum_{\Theta \in \{N, S, E, W\}} c^{\Theta_{ij}} \Delta_{\Theta} u_{i,j}. \tag{2.13}$$

Therefore, the steepest descent equation [43] that combines discretized diffusivities and divergence term becomes

$$u_{i,j}^{(n+1)} = u_{i,j}^{(n)} + \Delta t \left(\text{div}_{ij}^{(n)} - \lambda \frac{u_{i,j}^{(n)} - f_{i,j}^{(n)}}{(u_{i,j}^{(n)})^{\frac{1}{\alpha}} + \varepsilon} \right), \tag{2.14}$$

where

$$u_{i,j}^{(0)} = f_{i,j} = f(ih, jh), \quad u_{i,0}^{(n)} = u_{i,1}^{(n)}, \quad u_{0,j}^{(n)} = u_{1,j}^{(n)}, \quad u_{P,i}^{(n)} = u_{P-1,i}^{(n)}, \quad \text{and} \quad u_{i,Q}^{(n)} = u_{i,Q-1}^{(n)},$$

$1 \leq i \leq P, 1 \leq j \leq Q$ (P and Q define number of rows and columns in $u_{i,j}$ or $f_{i,j}$, respectively), and n denotes the iteration number; also, $h > 0$ represents the grid interval, and $\varepsilon > 0$ prevents degenerative solutions due to division by zero. During the iteration process, $u_{i,j}$ is gradually updated and improved until it attains the highest possible PSNR (peak signal to noise ratio) [44].

2.4 Experiments

The performance of our model was verified through a series of experiments, and empirical results were compared against those generated by classical models: traditional Perona–Malik [26], Adaptive Perona–Malik (Guo) [45], Charbonnier [40], Total Variation [28], Deep Neural Network (DNN) [46], and FFDNet [47]. The models were selected based on relevance, recency, and citation count. The DNN and FFDNet models, in addition, highlight the strength of our model relative to denoising models based on the deep neural network framework that have demonstrated promising outcomes [46, 48–51].

The first experiment aimed at evaluating the ability of different nonlinear diffusion models to protect critical image features while ensuring minimum noise in flat regions. Therefore, we applied the models on a synthetic image corrupted by speckle noise of density 0.05, sufficiently large amount of noise to discern the performance differences among the models under comparisons. Next, PSNR and MSSIM (mean structural similarity) [52] indices were applied to measure quality of the results. PSNR, defined by

$$\text{PSNR} = 20 \log \left(\frac{255}{\sqrt{\frac{1}{PQ} \sum (u - f)^2}} \right), \quad (2.15)$$

signifies the signal strength depicted by an image. Detailed images with minimum noise have higher PSNR values, and such images may be useful in various image processing tasks. On the contrary, MSSIM exploits the human visual system to describe the perceptual quality of the image. This metric follows the equation

$$\text{MSSIM} = \frac{(2\mu_u\mu_f + c_1)(2\sigma_{uf} + c_2)}{(\mu_u^2 + \mu_f^2 + c_1)(\sigma_u^2 + \sigma_f^2 + c_2)}, \quad (2.16)$$

where (μ_u, μ_f) and (σ_u, σ_f) denote means and standard deviations of u and f , respectively; σ_{uf} depicts the covariance between u and f ; and, c_1 and c_2 are stabilizing constants.

In the second set of experiments, the diffusion models were applied to natural SAR images¹ corrupted by noise with varied statistical distributions. Because of the unknown original images, we used the no-reference quality metric to assess the objective qualities of the restored images. This metric uses the von Mises distribution [53] with the probability density function defined by

$$f(\theta |_{\mu, \kappa}) = \frac{1}{2\pi I_0(\kappa)} e^{\kappa \cos(\theta - \mu)}, \quad (2.17)$$

where the variables and functions are defined as follows: $I_0(\kappa)$, modified Bessel function of order zero; θ , 2π -interval within the graph; μ , mean of the distribution; and, κ , shape-defining parameter of the von Mises distribution. The behavior of κ suggests that it can measure quality of an image. The value of κ increases with decreasing noise density. To further evaluate the performance of our method, another image quality assessment metric, called Equivalent Number of Looks (ENL) was used [54–56]. ENL, given by

$$\text{ENL} = \frac{(\text{mean})^2}{\text{variance}}, \quad (2.18)$$

is computed over a selected homogeneous region of an image and measures the despeckling capability of the method. Larger values of ENL signify effective removal of speckle noise in the image.

3 Results and discussions

Visual results show that the proposed model remains stable over a longer period. In essence, the output images generated by our evolutionary system exhibit higher perceptual qualities even when subjected to many iterations. Under this condition, other models (e.g. Total variation) perform poorly by generating nearly flat images (Fig. 2). Furthermore, PSNR and MSSIM values depicted by our model become fairly uniform after attaining global maxima (Fig. 3). This interesting behavior—which may be originated from a well-behaved energy functional—implies that the model guarantees

¹ <https://rslab.ut.ac.ir/data>.

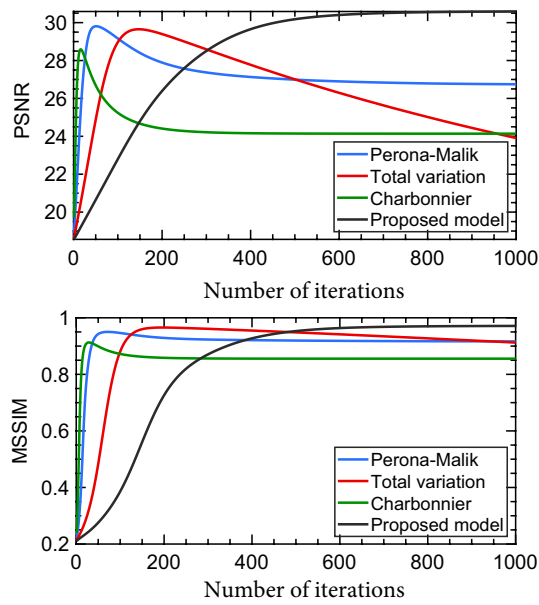


Fig. 3 Performance measures depicted by different denoising methods

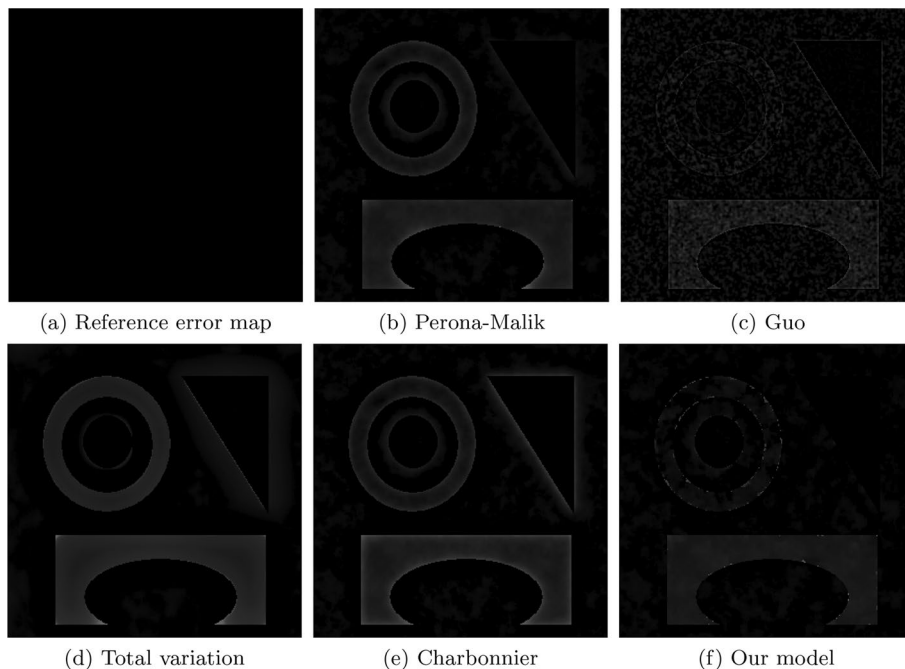


Fig. 4 Error maps generated by different denoising methods

appealing results irrespective of the iteration number. Figure 3 shows that other nonlinear diffusion models require manual tuning of the iteration number to achieve relatively convincing results—a process that is both inconvenient and inefficient.

Error maps (absolute difference between original and restored images) show that the proposed model produces minimum visible errors compared with other classical

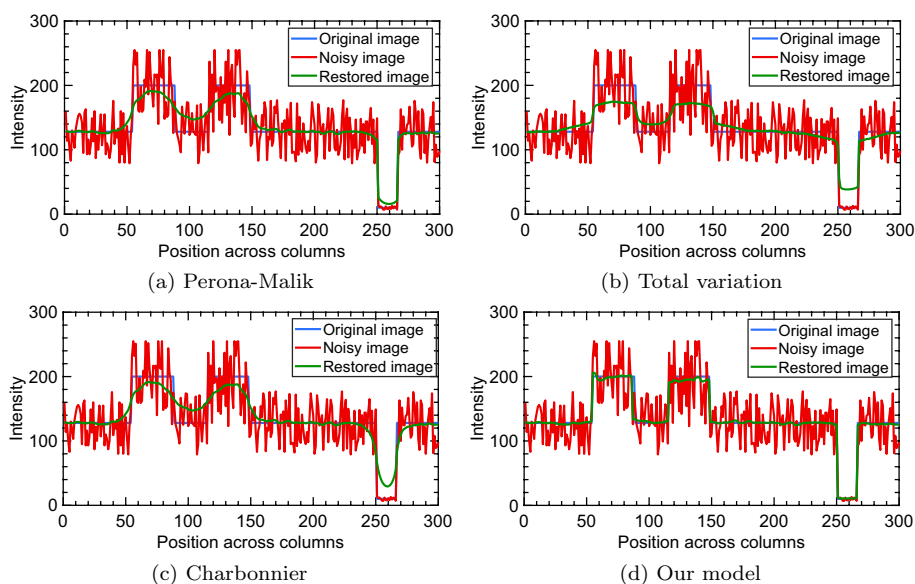


Fig. 5 Error maps generated by different denoising methods

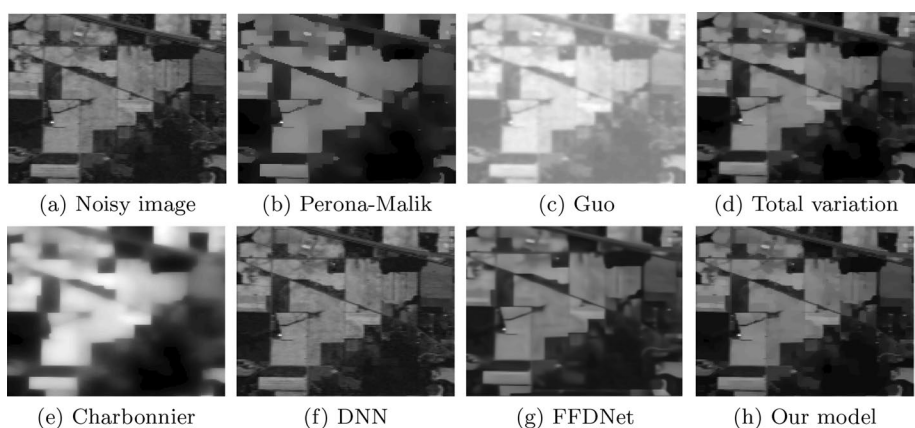


Fig. 6 Restored images by different models applied on the 180th-channel of the Indian pines dataset

models (Fig. 4). Therefore, we can assert that our model restores content-rich images containing the lowest amount of noise. The new regularization term was crafted specifically to deal with the nature of noise in SAR images (speckle or multiplicative), and this design strategy could partly explain one of the reasons for the outperformance of the proposed model.

Furthermore, the proposed model can recover critical image features and suppress noise more effectively (Fig. 5). Compared with some classical methods, our edge-locating functional traces edges and contours more accurately, and ensures revelation of stronger and clearer edges that promote visual perception. The edge-recovery capability of the proposed functional may be useful in machine-related tasks that demand detailed scenes to make informed decisions. Conversely, Perona–Malik and Charbonnier models smudge edges, and Total variation tends to reduce intensity of the output images.

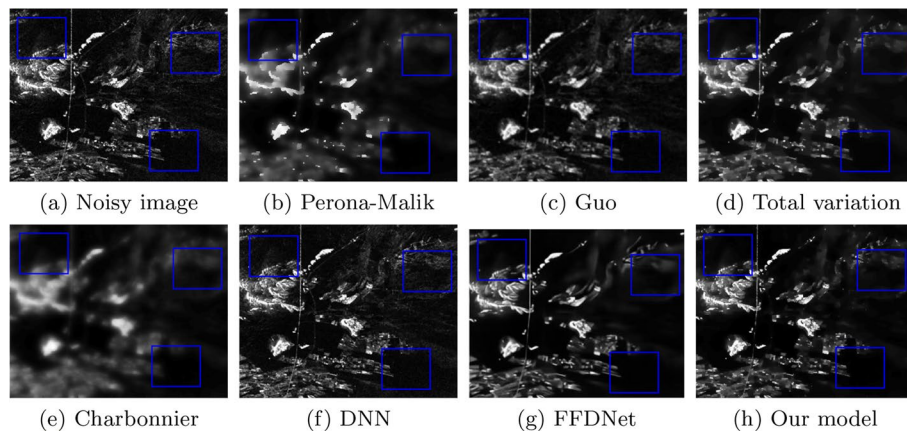


Fig. 7 Restored images by different models applied on the Salinity Soil SAR image

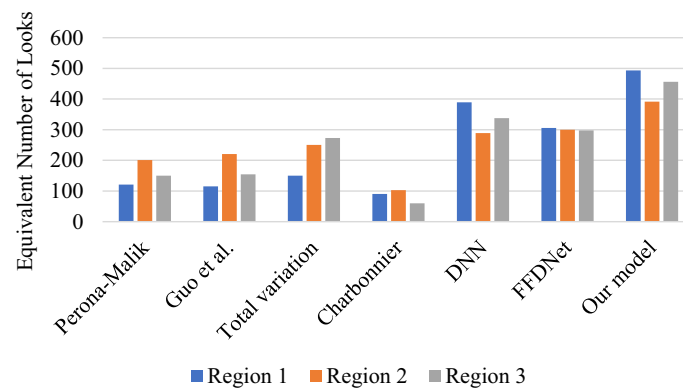


Fig. 8 Equivalent Number of Looks generated by different despeckling methods applied on the selected regions of an input image

Table 1 No-reference image quality values based on the von Mises distribution. (Images in the first, second, and third columns refer to specific channels in the Indian pines dataset)

Methods	von Mises distribution quality value					
	120 th -Channel	70 th -Channel	50 th -Channel	Washington	Soil Salinity	Las Vegas
Perona-Malik [26]	0.1168	0.1429	0.1292	0.3248	0.2951	0.1593
Guo [45]	0.1134	0.1133	0.1133	0.5539	0.4971	0.1445
Total variation [28]	0.1180	0.1414	0.1266	0.5017	0.3574	0.1659
Charbonnier [40]	0.1131	0.1190	0.1132	0.1799	0.1819	0.1130
DNN [46]	0.1229	0.1429	0.1292	0.5949	0.5366	0.1745
FFDNet [47]	0.3490	0.2421	0.2706	0.5751	0.4071	0.1867
Our model	0.1229	0.1443	0.1305	0.5708	0.4051	0.1745

Empirical results from natural SAR images demonstrate the efficacy of our diffusion model to suppress speckles (Figs. 6 and 7). The model retains naturalness of the images and encourages preservation of important features while optimally maintaining minimum speckle noise. Figures 6 and 7 show that the visual results produced by

our model are comparable with those produced by deep neural networks, which have been benchmarked by scholars that they outperform most of the available denoising models [46, 47].

Using the no-reference quality metric, based on the von Mises distribution, we found that the proposed nonlinear diffusion model generate higher quantitative values in several cases (Table 1). However, the quality values of our method are slightly lower than that of FFDNet. Despite this observation, perceptual qualities of the images generated by FFDNet seem lower than those defined by the proposed model (Figs. 6 and 7): FFDNet tends to oversmooth the images and to modify their contrast features.

Furthermore, ENL values generated by despeckling methods suggest that the proposed model outperforms in terms of its ability to suppress spurious details in flat image regions (Fig. 8). In essence, ENL results depicted by our method are comparable with those demonstrated by deep neural networks.

4 Conclusion

This work introduces a nonlinear diffusion model for suppressing speckles in SAR images. Driven by the compelling results depicted by our model, future studies may need to address critical questions in the area of image denoising. First, how can we derive an exact energy functional corresponding to the proposed diffusion model? Second, can our model be used in conjunction with the deep neural networks to further improve the denoising results? Third, how can the shape-defining constants of the proposed model be automatically tuned (perhaps by defining them as functions of the evolving solution, u)? Can denoising methods that have demonstrated superior performance in other applications [57–59] be adapted to address challenges in SAR imagery? Answers to these important questions may advance the current research and make the results impactful to a range of science and engineering fields.

Abbreviations

SAR	Synthetic radar aperture
PSNR	Peak signal to noise ratio
MSSIM	Mean structural similarity
DNN	Deep Neural Network
FFDNet	Feed-forward network

Acknowledgements

Not applicable.

Author contributions

All co-authors equally contributed in the research and production of the paper.

Funding

This work is not supported by any organization or institution.

Availability of data and materials

To allow other scholars reproduce our results, we have uploaded the implementation codes in the MATLAB File Exchange (https://www.mathworks.com/matlabcentral/fileexchange/74536-edge-aware-nonlinear-diffusion-driven-regularization-model?s_tid=srchtitle). Additional information regarding the proposed model, including experimental settings and variable/parameter definitions, can be found in the codes.

Declarations

Competing interests

The authors declare that they have no competing interests.

Received: 23 March 2020 Accepted: 28 December 2023

Published online: 11 January 2024

References

1. A. Moreira, P. Prats-Iraola, M. Younis, G. Krieger, I. Hajnsek, K.P. Papathanassiou, A tutorial on synthetic aperture radar. *IEEE Geosci. Remote Sens. Magazine* **1**, 6–43 (2013)
2. N. Bhatta, M. Geethapriya, RADAR and its Applications. In *IEEE Geoscience and remote sensing magazine* (2016)
3. A. Khmag, A.R. Ramli, S.A.R. Al-Haddad, S.J.B. Hashim, Additive and multiplicative noise removal based on adaptive wavelet transformation using cycle spinning. *Am. J. Appl. Sci.* **11**(2), 316–328 (2014)
4. Y. Murali, M. Babu, M.V. Subramanyam, M. Prasad, A survey on de-speckling of SAR images 1. *IJECT* **5**, (2014)
5. J. Glaister, A. Wong, D.A. Clausi, Despeckling of synthetic aperture radar images using monte Carlo texture likelihood sampling. *IEEE Trans. Geosci. Remote Sens.* **52**(2), 1238–1248 (2014)
6. W. Ni, X. Gao, Despeckling of SAR image using generalized guided filter with Bayesian nonlocal means. *IEEE Trans. Geosci. Remote Sens.* **54**, 1–13 (2015)
7. Y. Meng, Y. Liu, Z. Zhou, Q. Luo, A Speckle Reduction Model for Sar Images Based on Beltrami Regularization. *IGARSS 2018—2018 IEEE International Geoscience and Remote Sensing Symposium* 2358–2361, (2018)
8. Z. Yu, W. Wang, C. Li, W. Liu, J. Yang, Speckle noise suppression in SAR images using a three-step algorithm. *Sensors* **18**, 3643 (2018)
9. A. Meenakshi, V. Punitham, Performance of speckle noise reduction filters on active radar and SAR images. *Gopalax-Int. J. Technol. Eng. Syst. (IJTES)* **1**, 112–114 (2011)
10. A. Rajamani, V. Krishnaveni, Performance analysis survey of various SAR image despeckling techniques. *Int. J. Comput. Appl.* **90**(7), (2014)
11. D. Hazarika, V.K. Nath, M. Bhuyan, A lapped transform domain enhanced lee filter with edge detection for speckle noise reduction in SAR images. In *2015 IEEE 2nd International Conference on Recent Trends in Information Systems (ReTIS)*, IEEE, 243–248, (2015)
12. N. Devi, S. Sharma, Synthetic Aperture Radar (SAR) Images processing: a review. *Int. Res. J. Eng. Technol. (IRJET)* **3**, (2016)
13. S. Banerjee, S.S. Chaudhuri, A review on various speckle filters used for despeckling SAR images. In *2018 Second International Conference on Computing Methodologies and Communication (ICCMC)*, IEEE 68–73, (2018)
14. H.P. Leelavathi, D.J. Prakash, Effective speckle noise removal of SAR image based on combination of modified PCA and HMF with enhancement. *Int. J. Eng. Trends Technol.* **61**, 171–177 (2018)
15. X. Ma, P. Wu, H. Shen, A nonlinear guided filter for polarimetric SAR image despeckling. *IEEE Trans. Geosci. Remote Sens.* **57**(4), 1918–1927 (2018)
16. D. Suresh, N. Dhanalakshmi, V.N. Kumar, Removing speckle noise in synthetic aperture radar images using hybrid filtering. *Int. J. Pure Appl. Math.* **119**(15), 979–990 (2018)
17. X. Cao, Y. Ji, L. Wang, B. Ji, L. Jiao, J. Han, SAR image change detection based on deep denoising and CNN. *IET Image Proc.* **13**(9), 1509–1515 (2019)
18. F. Gu, H. Zhang, C. Wang, A two-component deep learning network for SAR image denoising. *IEEE Access* **8**, 17792–17803 (2020)
19. W. Ni, X. Gao, Despeckling of SAR image using generalized guided filter with Bayesian nonlocal means. *IEEE Trans. Geosci. Remote Sens.* **54**, 567–579 (2015)
20. Y. Zhao, J.G. Liu, B. Zhang, W. Hong, Y.R. Wu, Adaptive total variation regularization based SAR image despeckling and despeckling evaluation index. *IEEE Trans. Geosci. Remote Sens.* **53**(5), 2765–2774 (2014)
21. H. Choi, J. Jeong, Speckle noise reduction technique for SAR images using statistical characteristics of speckle noise and discrete wavelet transform. *Remote Sens.* **11**(10), 1184 (2019)
22. H. Yang, J. Li, L. Shen, J. Lu, A convex variational model for restoring SAR images corrupted by multiplicative noise. *Mathematical Problems in Engineering* 2020, (2020)
23. X. Ma, H. Shen, L. Zhang, PolSAR anisotropic diffusion filter with a refined similarity measure and an adaptive fidelity constraint. *Int. J. Remote Sens.* **37**(24), 5988–6011 (2016)
24. J. Fang, S. Hu, X. Ma, A boosting SAR image despeckling method based on non-local weighted group low-rank representation. *Sensors* **18**(10), 3448 (2018)
25. F. Catté, P.L. Lions, J.M. Morel, T. Coll, Image selective smoothing and edge detection by nonlinear diffusion. *SIAM J. Numer. Anal.* **29**, 182–193 (1992)
26. P. Perona, J. Malik, Scale-space and edge detection using anisotropic diffusion. *IEEE Trans. Pattern Anal. Mach. Intell.* **12**(7), 629–639 (1990)
27. B.J. Maiseli, N. Ally, H. Gao, A noise-suppressing and edge-preserving multiframe super-resolution image reconstruction method. *Signal Proc. Image Commun.* **34**, 1–13 (2015)
28. L.I. Rudin, S. Osher, E. Fatemi, Nonlinear total variation based noise removal algorithms. *Physica D* **60**(1–4), 259–268 (1992)
29. X. Shan, J. Sun, Z. Guo, Multiplicative noise removal based on the smooth diffusion equation. *J. Math. Imaging Vision* **61**(6), 763–779 (2019)
30. I. Artyukov, N. Irtuganov, Noise-driven anisotropic diffusion filtering for X-ray low contrast imaging. *J. Russ. Laser Res.* **40**(2), 150–154 (2019)
31. M. Gao, B. Kang, X. Feng, W. Zhang, W. Zhang, Anisotropic diffusion based multiplicative speckle noise removal. *Sensors* **19**(14), 3164 (2019)
32. D. Andrushia, N. Anand, P. Arulraj, Anisotropic diffusion based denoising on concrete images and surface crack segmentation. *Int. J. Struct. Integrity* (2019)

33. J. Bai, X.C. Feng, Image denoising using generalized anisotropic diffusion. *J. Math. Imaging Vision* **60**(7), 994–1007 (2018)
34. S. Nandal, S. Kumar, Fractional-order anisotropic diffusion for defogging of RGB images. *Int. J. Image Graphics* **20**(01), 2050001 (2020)
35. A. João, A. Gambaruto, R. Pereira, A. Sequeira, Robust and effective automatic parameter choice for medical image filtering. *Comput. Methods Biomech. Biomed. Eng. Imaging Vis.* **8**(2), 152–168 (2020)
36. A.R. Soheili, N. Mohamadi, F. Toutounian, A denoising PDE model based on isotropic diffusion and total variation models. *Comput. Methods Diff. Equ.* (2020)
37. J. Weickert, *Anisotropic diffusion in image processing*, vol. 1 (Teubner Stuttgart, 1998)
38. S. Kichenassamy, The perona–malik paradox. *SIAM J. Appl. Math.* **57**(5), 1328–1342 (1997)
39. J. Weickert, B. Benhamouda, *Why the Perona-Malik filter works* (Citeseer, 1997)
40. P. Charbonnier, L. Blanc-Feraud, G. Aubert, M. Barlaud, Two deterministic half-quadratic regularization algorithms for computed imaging. In *Proceedings of 1st International Conference on Image Processing*, Volume 2, IEEE 168–172, (1994)
41. H.P. Langtangen, *Finite difference methods for diffusion processes*. University of Oslo (2013)
42. R. Courant, K. Friedrichs, H. Lewy, On the partial difference equations of mathematical physics. *IBM J. Res. Dev.* **11**(2), 215–234 (1967)
43. J. Fliege, B.F. Svaiter, Steepest descent methods for multicriteria optimization. *Math. Methods Oper. Res.* **51**(3), 479–494 (2000)
44. Z. Wang, A.C. Bovik, Mean squared error: love it or leave it? A new look at signal fidelity measures. *IEEE Signal Process. Mag.* **26**, 98–117 (2009)
45. Z. Guo, J. Sun, D. Zhang, B. Wu, Adaptive Perona–Malik model based on the variable exponent for image denoising. *IEEE Trans. Image Process.* **21**(3), 958–967 (2011)
46. K. Zhang, W. Zuo, Y. Chen, D. Meng, L. Zhang, Beyond a Gaussian denoiser: residual learning of deep CNN for image denoising. *IEEE Trans. Image Process.* **26**(7), 3142–3155 (2017)
47. M. Tassano, J. Delon, T. Veit, An analysis and implementation of the ffdnet image denoising method. *Image Proc. Line* **9**, 1–25 (2019)
48. W. Jifara, F. Jiang, S. Rho, M. Cheng, S. Liu, Medical image denoising using convolutional neural network: a residual learning approach. *J. Supercomput.* **75**(2), 704–718 (2019)
49. Z. Yang, X. Zhuang, K. Sreenivasan, V. Mishra, T. Curran, D. Cordes, A robust deep neural network for denoising task-based fMRI data: an application to working memory and episodic memory. *Med. Image Anal.* **60**, 101622 (2020)
50. X. Li, J. Xiao, Y. Zhou, Y. Ye, N. Lv, X. Wang, S. Wang, S. Gao, Detail retaining convolutional neural network for image denoising. *J. Visual Commun. Image Representation* 102774 (2020)
51. C. Tian, Y. Xu, W. Zuo, Image denoising using deep CNN with batch renormalization. *Neural Netw.* **121**, 461–473 (2020)
52. Z. Wang, A.C. Bovik, H.R. Sheikh, E.P. Simoncelli, Image quality assessment: from error visibility to structural similarity. *IEEE Trans. Image Process.* **13**(4), 600–612 (2004)
53. S. Gabarda, G. Cristóbal, No-reference image quality assessment through the von Mises distribution. *JOSA A* **29**(10), 2058–2066 (2012)
54. S.N. Anfinsen, A.P. Doulgeris, T. Eltoft, Estimation of the equivalent number of looks in polarimetric synthetic aperture radar imagery. *IEEE Trans. Geosci. Remote Sens.* **47**(11), 3795–3809 (2009)
55. G. Di Martino, M. Poderico, G. Poggi, D. Riccio, L. Verdoliva, Benchmarking framework for SAR despeckling. *IEEE Trans. Geosci. Remote Sens.* **52**(3), 1596–1615 (2013)
56. H. Xie, L.E. Pierce, F.T. Ulaby, SAR speckle reduction using wavelet denoising and Markov random field modeling. *IEEE Trans. Geosci. Remote Sens.* **40**(10), 2196–2212 (2002)
57. C. Yan, B. Shao, H. Zhao, R. Ning, Y. Zhang, F. Xu, 3d room layout estimation from a single rgb image. *IEEE Trans. Multimedia* (2020)
58. C. Yan, Z. Li, Y. Zhang, P. Qin, X. Ji, Q. Dai, Depth image denoising using nuclear norm and learning graph model. *IEEE Trans. Multimedia* (2019)
59. C. Yan, B. Gong, Y. Wei, Y. Gao, Deep multi-view enhancement hashing for image retrieval. *IEEE Trans. Pattern Anal. Machine Intell.* (2020)

Anthony Bua is currently pursuing Master of Science in Telecommunication Engineering at the Department of Electronics and Telecommunications Engineering, University of Dar es Salaam. In 2014, he completed his Bachelor's Degree in Computer Engineering from the College of Engineering, Design, Art and Technology at the University of Makerere, Uganda. His research interests include image processing and wireless communication. Mr. Anthony is the current technical officer/consultant at a non-government organization, Kampabits.

Goodluck Kapyela is a Tutorial Assistant in the Department of Electronics and Telecommunications Engineering, College of Information and Communication Technologies, University of Dar es Salaam. He acquired Bachelor of Science in Electronics Science and Communication from the University of Dar es Salaam in 2013. Currently, he is pursuing Master of Science in Electronics Engineering and Information Technology from the same University. His research interest includes Digital Image Processing and Machine learning.

Libe Massawe is a Lecturer in the Department of Electronics and Telecommunication Engineering. She completed her Bachelor degree in Electrical Engineering at the University of Dar es Salaam in 2002, Master

of Science in Electrical and Electronics Engineering at University of the Ryukyus in Japan in 2005 and PhD in Electrical Engineering at Central University of Technology, Free State South Africa in 2012. She is involved in teaching and supervising undergraduate and postgraduate students and carrying out research and consultancy activities in the field of ICT. She has taught undergraduate and postgraduate courses in Digital and Analogue Electronics, Control Engineering, Digital Telecommunication and Sensors and Microsystem Engineering. Her research interest includes RFID, Sensor networks and Wireless communication. She has supervised a number of Bachelor and Masters students and she has examined a number of Masters and PhD thesis and dissertations. Dr Libe Massawe is the current Head of Department of Electronics and Telecommunication Engineering at UDSM.

Baraka Maiseli earned his Doctoral degree in 2015 from the Harbin Institute of Technology (HIT), PR China, where he was also awarded the honorary certificate as the best international scholar of the year. Between 2015 and 2017, he worked with HIT as a postdoctoral researcher. Maiseli has published several articles in referred Journals, and is a verified peer reviewer for various international journals: IEEE Transactions on Industrial Electronics, Neurocomputing, IET Biometrics, Signal Processing, and International Journal of Remote Sensing, among others. His research interests are in machine learning, computer vision, image and video processing, artificial intelligence, and embedded electronics. Currently, Maiseli works at the University of Dar es Salaam (UDSM), Department of Electronics and Telecommunication Engineering, as a lecturer. With more than 13 years of teaching experience at UDSM, Maiseli has been supervising both undergraduate and postgraduate students in their projects, research, and practical training.

Submit your manuscript to a SpringerOpen[®] journal and benefit from:

- ▶ Convenient online submission
- ▶ Rigorous peer review
- ▶ Open access: articles freely available online
- ▶ High visibility within the field
- ▶ Retaining the copyright to your article

Submit your next manuscript at ▶ [springeropen.com](https://www.springeropen.com)
